Minimalist Jumping Robots for Celestial Exploration

Joel Burdick and Paolo Fiorini

The International Journal of Robotics Research 2003; 22; 653
DOI: 10.1177/02783649030227013

Joel Burdick

Mechanical Engineering
California Institute of Technology
Pasadena, California 91125

Paolo Fiorini

Dipartimento di Informatica
Universitá di Verona
Verona, Italy 37134

Minimalist Jumping Robots for Celestial Exploration

Abstract

In this paper we describe a novel approach to the design and deployment of small and minimally actuated jumping or hopping robots that are suitable for exploring the unstructured terrains of celestial bodies. We introduce the basic jumping mobility paradigm, as well as the evolution of our hopping robot concept by way of the main prototypes that we have developed. These prototypes show that a small number of actuators can control the vehicle's steering, hopping, and self-righting motions. The last prototype is equipped with wheels so that precision motion can be combined with gross hopping motion. Lessons learned during the development of these prototypes have general applicability to the design of jumping robots. In addition to reviewing the issues relevant to the design of jumping systems, in this paper we describe some of the key mechanisms that enable our approach, we summarize tests obtained with these systems, and we present our future plans of localization and sensing for hopping mobility.

KEY WORDS—planetary exploration, field robot, planetary robot, hopping robot, nano rover

1. Introduction and Motivation

In this paper we introduce, analyze, and experimentally explore a new "jumping" or "hopping" paradigm for robot mobility. We are motivated to develop this approach by the recent trend toward smaller and more frequent space missions to Mars and other celestial bodies such as moons, asteroids, and comets. These celestial bodies are usually characterized by a low to medium gravitational environment and unstructured terrain. The potential for such missions has sparked new interest in multi-functional vehicles, capable of providing high mobility for scientific packages in complex terrains. The space exploration community has spent considerable effort and has significant ongoing interest in the development of mechanical mobility systems that are capable of supporting scientific exploration of such bodies.

The work described in this paper arises from an obvious debate about the best way to design exploratory robotic systems under the very severe constraints on launch mass. For a given amount of launch mass (100 kg for example), is it preferable to have one or two exploratory vehicles (weighing 50 or 100 kg in this example), or many small vehicles (e.g., 50 2 kg mass vehicles), or one large vehicle with many small helpers (e.g., a 50 kg vehicle with 25 2 kg assistants)? To date, the Pathfinder mission to Mars and the Mars exploration missions planned for the next decade have focused on the single vehicle paradigm. The work presented in this paper represents a preliminary proof-of-concept study of one mobility concept that can be useful for implementing alternative design paradigms that employ many lightweight vehicles. To understand the motivation for our approach, we first briefly review the main planetary mobility paradigms that have been investigated to date in terms of their ability to overcome obstacles and their inherent mechanical complexity.

To date, the only successfully deployed mobility paradigm for autonomous exploration of planetary surfaces is a six-wheeled rover, as seen in the Pathfinder mission's Sojourner vehicle (Mishkin et al. 1998), and in proposed Mars exploration missions planned for the next decade. Because of its unique rocker-bogey suspension, a six-wheeled rover of the Sojourner type can traverse obstacles that are about 1.5 times the vehicle's wheel diameter. However, this still represents only a fraction of the vehicle's overall body length. Moreover, this design relies upon a significant number of actuators and complex suspension linkages. For example, the Sojourner mobility system used ten motors, while prototypes for planned Mars missions use twelve independent actuators (Volpe 1999). Inflatable wheels may be able to overcome somewhat proportionally larger obstacles. Nonetheless,

The International Journal of Robotics Research
Vol. 22, No. 7–8, July–August 2003, pp. 653-674,

wheeled designs have fundamental limitations on the obstacle size, compared to body length, that can be overcome. Thus, some terrains are not accessible to wheeled vehicles. Terrain accessibility may become a problem as vehicles are scaled down in size in order to enable multi-vehicle design approaches. Researchers at the Jet Propulsion Laboratory (JPL) have successfully demonstrated small (∼1 kg mass) four-wheeled exploratory rovers in realistic simulated conditions (Welch, Wilcox, and Nasif 1998). However, because of the fundamental limitations imposed by wheels, these vehicles can only go over obstacles a few centimeters in height.

Legged robots can overcome the limited traversability of wheeled vehicles in many rugged terrains. Legged rovers have previously been proposed for Lunar and Martian exploration (Bares et al. 1989), and large legged vehicles have been demonstrated in the tough environment of an Alaskan volcano (Bares and Wettergreen 1999). While legged robots can potentially access rough terrains, they are mechanically complex, requiring numerous joints, actuators, and linkages. While spiders and insects can demonstrate impressive ability to climb over obstacles, it is not yet clear that multi-legged robot vehicles have impressive ability to overcome large obstacles when they are scaled down in size.

As discussed above, even wheeled rover vehicles use a significant numbers of actuators and complex suspension linkages. Hence, most actively explored paradigms for planetary mobility are based on a large number of actuators and complex suspension linkages. There are a number of obvious drawbacks to using many motors and their associated linkages: an inherent risk in system failure; a need for larger power supplies and/or solar cells; a need for complex power electronics; and increased system weight (which reduces the weight that can be allocated to science payloads).

In this paper we explore another paradigm. Clearly, small vehicles operating in complex terrains may have to overcome obstacles which are equal to, or larger than, the vehicle's size. Vehicles that can vigorously "jump" or "hop" as part of their operation might be able to overcome such relatively large obstacles if they can reliably survive the hard landings inherent in the jumping process. The discussion in Sections 2 and 7.1 also shows that, as the magnitude of gravity is reduced, the practical efficiency of hopping increases relative to wheeled vehicles. Hence, hopping can be a realistic alternative to wheels in lower gravity environments. These simple observations motivate one part of our research program—the use of leaping motions for small robots in unstructured terrains. The operation of our hopper, which is described below, is more akin to the movement of a frog, rather than the oscillatory behavior of well-known hopping robots (Raibert 1986).

The second part of our research program is to explore "minimalist" approaches to mobility subsystem design that are aimed at minimizing the number of required mobility system actuators. Reducing the number of actuators is an attractive goal for planetary vehicle design, since such designs are likely to be smaller and lighter, with lower risk of failure. With significantly reduced size/mass, there is a greater likelihood that several rovers could be deployed in a single rocket launch payload. Furthermore, engineering motors for the frigid environment of deep space is a difficult task.

In summary, our goal is to develop small minimally actuated jumping devices. A truly minimally actuated device may not have the functionality necessary to carry out meaningful tasks. The research presented in this paper explores the trade-offs between functionality and complexity in the context of the design and development of a simple hopping robots. As an example of the benefits of our approach, our second generation hopping design demonstrates that a single actuator is enough to propel, steer, and self-right a simple hopper. The same actuator can also pan an on-board camera. Furthermore, the entire system weighs less than 1.3 kg, and efficiently converts stored energy to hopping motion. This system has demonstrated leaps of ∼12–15 body lengths. Hence, our single actuation design offers surprising capability, compactness, and efficiency.

Our work suggests that these jumpers may be a useful addition to the planetary rover family (e.g., they may operate in tandem with conventional rovers). They may also be suited for the cooperating behaviors planned for the next phases of Mars exploration, wherein many simple devices will coordinate their motions to collectively gather distributed scientific data over large areas.

After summarizing relevant prior work below, in Section 3 we describe the goals and issues that constrained our development. In Section 4 we describe the first ("generation one") prototype, while in Section 5 we summarize the performance of this system and its shortcomings. The lessons learned from this system led to the second generation system *the frogbot*, whose design and performance are described in Sections 6 and 7. There are, however, two main limitations with our second generation prototype, which may prevent its use in real exploration missions. They are fine motion control and navigation planning. The former refers to the robot's capability of accurately controlling its trajectory after landing and accurately reaching science targets. The latter refers to the robot's ability to precisely locate itself after each landing. The third generation prototype, the *Wheeled Hopper*, is described in Section 8. Our current research in the areas of navigation and planning for hopping robots is briefly described in Section 9. Finally, in Section 10 we summarize the main aspects of our research on hopping mobility and present our plans for future research in this area, including the present plans for our fourth generation vehicle.

2. Relation to Prior Work

Hopping systems for planetary mobility were first proposed in Oberth (1959) and Seifert (1967) as a promising trans-

portation concept for astronauts in a lunar environment. A first-order analysis of lunar hopper performance is presented in Kaplan and Seifert (1969). The authors propose a single-seat device propelled by a gas actuated leg hinged under the astronaut seat and stabilized by four elastic legs. The acceleration intensity and duration is limited by the tolerance of the human body. Automatic re-orientation of the hopper is not supported in this design concept. A two-seat hopping laboratory which is capable of changing direction during the stance phase is also briefly discussed. Based on data from the Apollo missions, the paper also compares different approaches to lunar transportation, showing that hopping can be an efficient form of transportation in a low-gravity environment. None of these conceptual studies was reduced to practice.

More recently, a hopping robot, whose structure is the precursor for some aspects of our first generation device, has been described in Lorigo et al. (1997). To our knowledge, the proposed device did not realize an experimental demonstration. The common characteristic of these two hopping systems is motion discontinuity, since a pause for re-orientation and recharge of the thrust mechanism is inserted between jumps. Motion discontinuity is common to all of the systems described in this paper.

Laboratory demonstrations of hopping robots have generally focused on continuous motion and dynamic stability, without pauses between jumps. Raibert's seminal work in this area is summarized in Raibert (1986), and analyzed mathematically in several works, such as Koditschek and Bühler (1991), Li and Montgomery (1990) and M'Closkey and Burdick (1993). In contrast to our design, these hoppers required the coordinated action of several actuators for propulsion and stabilization.

Research of non-holonomic systems has motivated a renewed interest in the control of hopping robots. An often analyzed device is the "Acrobot", a reversed double-pendulum with a single actuator located in the joint and free to move its base (Berkemeier and Fearing 1998; De Luca and Oriolo 1998; Hauser and Murray 1990; Spong 1995). Berkemeier and Fearing (1998) describe how to make the Acrobot jump by accelerating its center of mass until the base loses ground contact. The Acrobot's landing attitude is controlled by compensating for the robot's non-zero angular momentum at lift-off with in-flight rotations of the lower link. While the Acrobot uses only one actuator, it is only capable of motion on the vertical plane. In contrast, our single motor second generation hopper is not restricted in its motions.

The closest relevant work to ours comes from the impressive "scout" robot development program at the University of Minnesota (Budenske et al. 2000). The scout is a small two-wheeled vehicle containing a leaf spring whose deployment can cause the scout to leap a small distance for purposes of jumping up one stair or overcoming obstacles. The scout was designed for operation in indoor environments—its two wheels and low ground clearance are mainly suited for movement on smooth floors. In contract, we are targeting outdoor environments. Furthermore, the scout vehicle can hop a few body lengths, whereas our second generation hopper has achieved hops of 12–15 body lengths.

In the last few years, smaller wheeled rovers for planetary exploration have been designed and fabricated in several research laboratories. The interest in these systems is motivated by the fact that they can be effectively used in tandem with larger rovers to increase exploration range. The *Nanorover* developed at the National Aeronautics and Space Administration (NASA) JPL (Welch, Wilcox, and Nasif 1998) consists of a body (with approximate dimensions of $15 \times 15 \times 5$ cm^3) equipped with four movable struts each carrying a 6 cm wheel equipped with an internal motor and with helical cleats for skid steering. The movable struts in theory can be used to implement a jumping behavior, although only in the microgravity environment of an asteroid.

Other researchers have also explored minimalist approaches to mobility, although not in the context of jumping. For example, Bhattacharya and Agrawal (2000) and Bicchi et al. (1997) have presented designs, algorithms, and experimental data on small spherical rolling vehicles that are driven by two motors via a non-holonomic effect. While they only use two motors, these devices can only work on nominally flat terrain.

An earlier prototype of the first generation rover described in Section 4 is presented in more detail in Fiorini et al. (1999). We briefly summarize this system for a few reasons. First, we report on experimental results that were not presented in Fiorini et al. (1999). Secondly, some of the computing, electrical, and sensing subsystems are the same in both generations, and thus need only be discussed once. Most importantly, lessons learned from and evaluation of this system motivate the improved version described in Section 6, and provide some general lessons for the design of jumping vehicles.

3. Minimalist Hoppers: Operating Constraints and Approach

In this section we describe the practical constraints which drive our approach, along with an intuitive overview of the minimalist jumping cycle.

3.1. General Design Goals and Operating Assumptions

Our design and development program is driven by the desire to: (1) minimize the total number of system actuators; (2) minimize the overall size and weight of the entire package so that multiple rovers can be deployed; (3) carry a television camera and some simple on-board scientific sensors; and (4) achieve sufficient mobility to realize some useful scientific capabilities. The system should be able to carry enough on-board energy storage, combined with solar-cell assistance, to

enable a useful mission lifetime of weeks or months. Hence, energy efficiency must be of some concern.

The hopper must operate in terrain that ranges from sand to hard rock, and whose topography is unpredictable and varied. The mechanism must achieve a statically stable, steady-state posture between jumps for the purposes of camera image acquisition and scientific measurements. We assume that the vehicle is operating in a moderate gravitational environment, such as Mars (where gravity is about one third that of Earth). Micro-gravity environments (such as on asteroids) present additional requirements, as we must additionally insure that the hopper does not exceed escape velocity during lift-off. "Micro" wheeled rovers have been proposed for such environments (Welch, Wilcox, and Nasif 1998).

3.2. The Minimalist Hopping Cycle

The simultaneous control of hopping height, hopping direction, hopper stability, and camera pointing would require several actuators and complex coordination of the motions. To reduce the number of on-board actuators, we take a two-pronged approach. First, we describe a "minimalist hopping cycle" wherein as many operations as possible are scheduled sequentially, instead of simultaneously. Said differently, the minimalist hopping cycle consists of a sequence of disjoint or discontinuous motions that need not be actively coordinated. In this way, a single actuator can often be used to drive several operations in the sequence. Otherwise, the simultaneous control of these operations would require multiple actuators. Secondly, we try to obtain further reductions by mechanically multiplexing some actions, as described below.

The minimalist hopping operational cycle can be roughly broken down into the following actions, with this sequence representing one potential ordering of the operations:

(1) orient (steer) the body in the desired direction, in preparation for take-off;

(2) adjust hopping parameters (such as take-off angle);

(3) thrust (release stored energy);

(4) free flight;

(5) crash-land;

(6) self-right the mechanism after landing;

(7) pan the camera to acquire images;

(8) deploy scientific instruments as necessary, using fine mobility if available;

(9) recharge the thrusting mechanism (in preparation for the next jump);

(10) go to step (1).

Some of the actions can be ordered differently in the sequence, and some may be carried out in parallel. As shown in the discussion of our prototypes below, this sequence may be implemented in various ways and with different mechanisms.

The other key feature of our approach is the use of a pair of over-running (or one-way) clutches to multiplex the output of one motor to drive two separate functions. That is, a motor can be connected to two output shafts, as shown in Figure 1. When the motor is running clockwise, one output shaft is energized to drive a given function or subsystem, while its output to the other is disengaged. Changing the direction of the motor output then switches on the second subsystem, while disengaging the first. Such a scheme can be used whenever two different operations can be driven in a unidirectional fashion.

The following sections articulate, via a sequence of prototypes, how these simple ideas can be put into practice. In Section 4 we describe the initial prototype, which used only one motor for its operation and some obvious design choices. In Section 5 we discuss the shortcomings of some of the obvious design principles used in the first prototype. These observations provide some general guidelines for jumping robot design. In Section 6 we describe our second generation design, which still employs a single motor, but whose performance is quite superior to the first prototype. In Section 8 we describe a three-motor design to test a combination of jumping and wheeled mobility. In Section 10 we summarize our findings, and describe the current plans for our fourth generation prototype.

4. The First Generation Design

Figure 2 depicts the essential internal components of the first generation design. A clear polycarbonate shell surrounds the mechanism, and is attached to the body at the upper support and lower plate, as is shown in Figure 3. The shell is a "crash cage" which protects the mechanism during crash landings. Its transparency allows the internal camera to collect images. Control of the vehicle by a single actuator is implemented with the aid of an over-running clutch, as suggested in Section 3.2. With the decoupling action of the clutch, rotation of the motor in one direction drives the leg compression and leg release subsystem, while rotation in the other direction drives the camera rotation. Figure 4 schematically depicts the relative phasing and motor rotations for each operation described below.

Vertical hopping motions are generated by the release of a simple linear spring, which is compressed after each jump via a ball screw that is driven by the motor. The spring housing consists of two concentric cylinders that guide the spring's compression/decompression. The compressed spring is held in place by a spring-loaded ball bearing lock-release mechanism (Fiorini et al. 1999). This mechanism locks after a fixed amount of spring compression is reached. A few extra motor rotations beyond the locking point causes the mechanism to

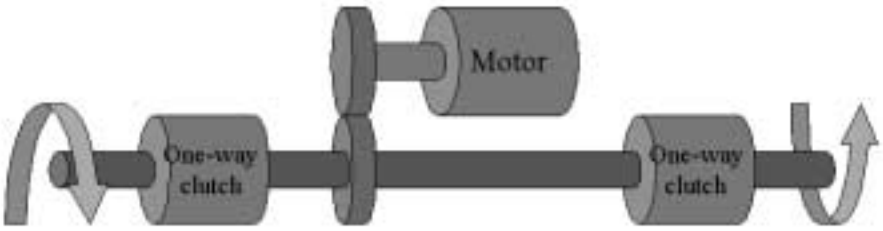

Fig. 1. Schematic diagram of the mechanical multiplexing scheme.

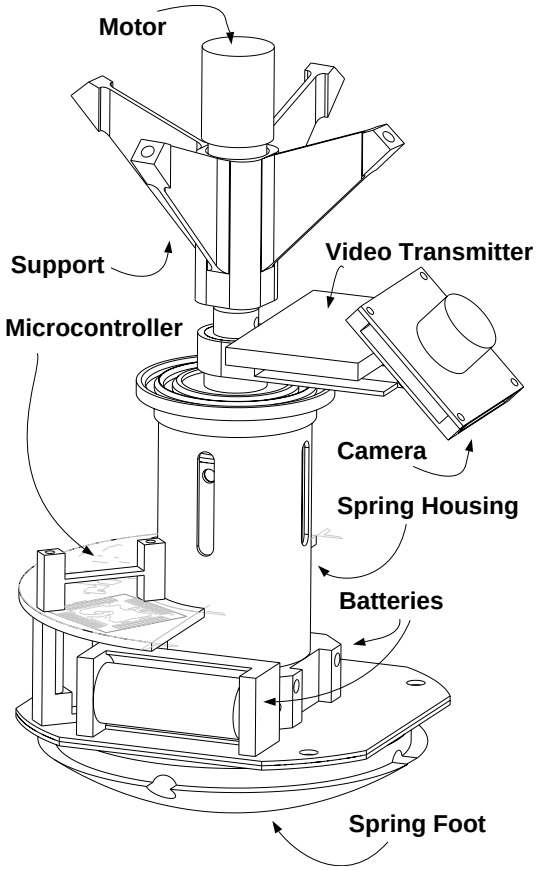

Fig. 2. Schematic diagram of the first generation mechanism. The surrounding polycarbonate shell is omitted for clarity.

Fig. 3. Photograph of the first generation system.

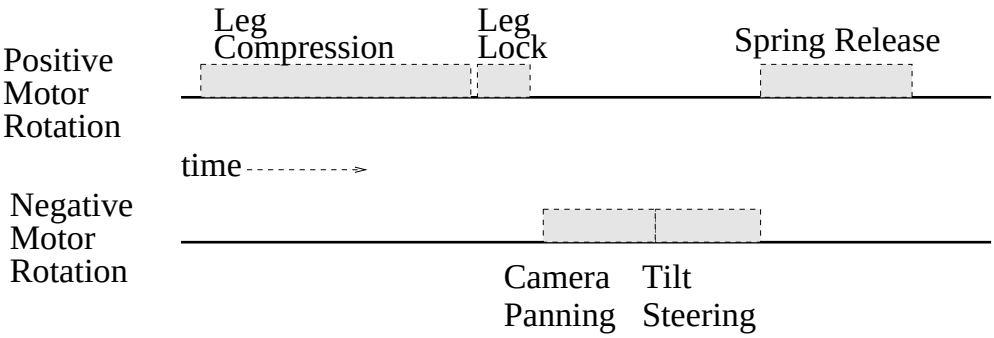

Fig. 4. Relative timing of the operations driven by the single driving motor.

release. By reversing the motor rotation, a camera can be rotated so as to take images through the clear shell. The body's orientation can also be modified by rotating the camera, whose off-axis center of mass causes the vehicle to tilt. Steering (the act of pointing the vehicle in the desired direction before take-off) is achieved via this concept by tilting the vehicle in the desired direction prior to launch. Since the camera is an off-center mass, the tilting is achieved by pointing the camera in the desired hopping direction. The self-righting capability is implemented passively in this design by creating a low center of mass—all of the batteries and heavy components are concentrated in the "bottom" of the hopper. The hopper takes off, flies, and lands with the bottom downward.

The electronic subsystem consists of a micro-controller board that contains a PIC CMOS microprocessor, motor controller and power circuits, communication ports, and analog/digital signal acquisition. The board consumes ∼0.35 Watts, excluding motor and science instruments. Additionally, the major board components have power-down features to conserve energy. Power is provided by four 12 V batteries. The video micro-camera broadcasts images on channel 14 by an RF transmitter.

The main dimensions of the robot are as follows: mass of the lower body, 575 g (including lower shell, batteries, foot, spring assembly, and electronics); mass of the upper body, 200 g (including upper shell, motor, bracket, and bearings); off-axis mass, 65 g (including camera, camera mount, arm, and transmitter); the length of the main axis of the hopper is 200 mm, the off-axis mass is 45 mm away from the axis and the minor axis of the body is 150 mm.

5. First Generation Post-Mortem

A number of tests were performed to assess this first design. We first focus on its jumping ability, and then summarize other useful observations. Even after experimental optimization of the thrust spring, this prototype only realized vertical jumping heights of about 80 cm and horizontal leaping distances of 30–60 cm. We determined that most of the energy that was stored in the spring was not converted to motion during the launching process. Let η be the "conversion efficiency" of a hopper that is propelled by decompression of an elastic member:

$$\eta = \frac{\text{hopper kinetic energy at takeoff}}{\text{energy stored in compressed member}} \times 100\% .$$

This number assesses how well a given hopping system converts elastic energy stored in the compressed member into actual hopper motion. The kinetic energy at lift-off can easily be inferred by the realized hopping height and distance. The stored energy is computed from the spring's compression and stiffness constant.

Our experiments have shown that the hopper achieves only a 20% efficiency, i.e., 80% of the energy stored in the spring is not converted into hopper motion. Instead, this energy is dissipated by friction and wasted motions of the mass–spring thrusting system. Clearly, such an energy loss is unacceptable for space missions. A large number of factors, such as internal dissipation of the spring material as well as friction in the moving and locking mechanisms, each contributed to this dissipation. However, three factors dominated the losses. First, at the end of decompression phase, the foot abruptly stops in an elastic impact with a mechanical stop, thereby dissipating its kinetic energy. The magnitude of this loss is proportional to the ratio of foot mass to total mass. In this design, the loss equals 15% of the spring's stored energy. Clearly, we should always reduce the foot mass to minimize this loss in this design, and all designs where the motion of an extending part is checked by a mechanical stop.

To understand the other factors, note that the total energy realized by leg decompression during lift-off is

$$E = \int_{t_i}^{t_{off}} F_R V_h \, \mathrm{d}t \qquad (1)$$

where F_R is the net wrench on the hopper due to the ground reaction force that is generated by the leg thrust, and V_h is the velocity of the hopper's center of mass. Spring decompression starts at time t_i, and the hopper breaks ground contact at t_{off}. For a lossless linear spring, $F_R = k_l \Delta x$, where k_l is the spring constant and Δx is the deviation from the unsprung length. In reality, F_R is reduced by loss mechanisms. Because the hopper tilts in order to steer, the ground reaction force is often not normal to the surface, and may fall outside the Coulomb friction cone. In this case, slippage and energy loss occurs during take-off. The horizontal component of F_R is bounded by the Coulomb law. Equation (1) says that the more the leg thrust force exceeds the Coulomb limit, the greater is the percentage energy loss. Such slipping was observed in our trials.

While the losses outlined above are obvious, the following is more subtle, and involves an inherent problem in the use of linear springs for hopping. Consider the behavior of eq. (1) during the decompression phase of the simple model in Figure 5(a). In the model, let M be hopper mass and k_l the leg stiffness. Ground compliance is crudely modeled with a spring of stiffness k_g. Let $k_c = (k_g^{-1} + k_l^{-1})^{-1}$. If $x(t)$ denotes vertical displacement of the hopper's center of mass from the ground plane, a simple analysis shows that during the lift-off phase:

$$x(t) = l_0^{'}(1 - \cos(\omega t))$$

where $l_0^{'} = l_0 - Mg/k_c$ and $\omega = \sqrt{k_l/M}$. Here g is the gravitational constant and l_0 is the amount of spring compression at thrust onset. Neglecting frictional and other losses summarized above, substitution of $F_R = k_g(l_0 - x(t))$ and $V_h = \dot{x}(t)$ into eq. (1) yields the kinetic energy delivered to the hopper by the leg thrust as a function of time:

$$E(t) = \frac{k_l (l_0^{'})^2}{4} [1 - \cos(2\omega t)] . \qquad (2)$$

In the idealized case, the hopper will lift off when $x(t_{off}) = l_0^{'}$, i.e., when $t_{off} = \frac{\pi}{2\omega}$. At this idealized lift-off time, eq. (2) yields the expected result that all of the spring's potential energy is converted into kinetic energy. Figure 6 plots eq. (2) versus time during the lift-off phase. Note that more of the kinetic energy is realized during the latter part of the decompression cycle, i.e., while F_R assumes a large value at the beginning of lift-off, V_h is small. Consequently, the integrand of eq. (1) is initially small.

Should the hopper prematurely leave the ground before the spring is fully extended, part of the spring's stored energy will not be usefully converted to kinetic energy. In fact, Figure 6 implies that *premature lift-off* is particularly bad for linear springs, where more of the useful work is realized near the end of the decompression cycle. A more sophisticated analysis of this problem, which includes the ground compliance and the non-linear coil spring phenomena known as *surge* (Shigley and Mischke 1989), suggests that the linear spring

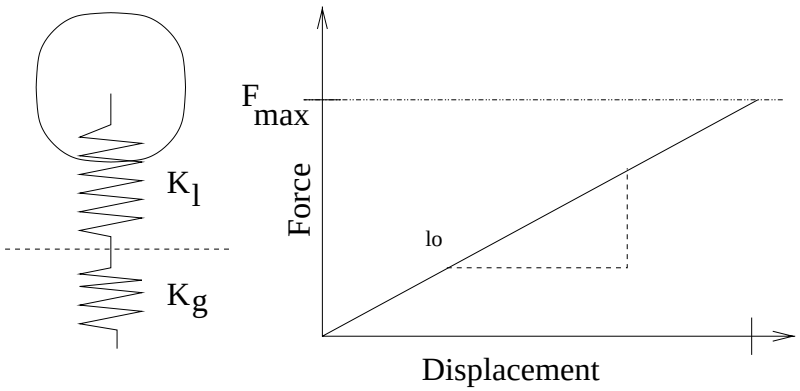

Fig. 5. (a) Simplified model. (b) Reaction force versus leg displacement for first generation thrust spring.

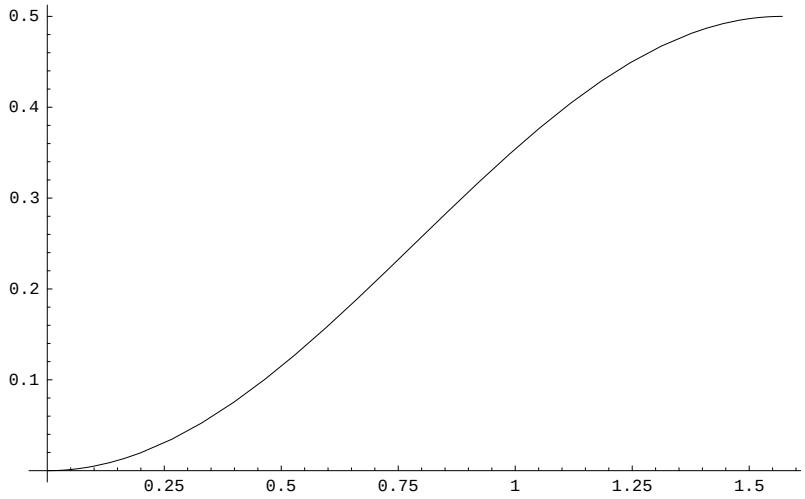

Fig. 6. Plot of realized kinetic energy (in units of $k(l_0')^2$) versus time for idealized linear spring ($\omega = 1$).

can often experience premature lift-off, thereby limiting the conversion of stored energy to hopping motion. Moreover, the more that F_R exceeds Mg at the beginning of the thrust, the greater is the likelihood of premature lift-off. Thus, we might naively increase the spring stiffness in an attempt to increase the launching force. However, this greater spring stiffness also increases the likelihood of premature lift-off, and hence energy loss. Such premature lift-off was observed in some of our experiments.

Figure 5 also suggests another deficiency in the linear spring design. The motor's peak design torque is determined by the spring force at maximum compression, F_{max}. Given the discussion above, we can conclude that most of the motor's design torque is required to compress the spring in a regime where it does little good.

Besides inefficiency, the first generation design had other drawbacks. First, the passive self-righting system will clearly not work in many terrains, and is therefore not robust, i.e., if the vehicle landed on hard ground, and subsequently tumbled onto a sandy spot, it could have become irretrievably stuck on its side in the soft sand. Secondly, the steering system was not reliable. Again, in soft ground, the rotation of the off-axis camera did not reliably cause the body to tilt in the desired direction.

6. The Second Generation Design

The goal of the second generation design was to solve the three major shortcomings of the first generation system: (1) inefficient hopping; (2) unrobust steering; (3) unrobust self-righting capability. We were able to realize all of these objectives while still using only a single actuator. To overcome these shortcomings of the first generation design, this generation uses an active steering mechanism, an active self-righting system, and a novel energy storage/thrusting system. Each of these subsystems is described below.

Fig. 7. Schematic view of the second generation hopper, showing some key components.

Figure 7 shows a schematic diagram of the second generation design, while Figure 8 shows a photograph of the second generation system in its uncompressed state, and Figure 9 shows the vehicle in its compressed state. In its compressed state, the robot fits into a roughly $15 \times 15 \times 15$ cm^3 space. Its total weight, including battery pack, is approximately 1.3 kg.

6.1. Energy Storage and Thrusting Mechanism

The need for improved energy conversion efficiency led us to consider different means for storing and releasing mechanical energy. While we considered gas expansion, linear impulsive actuators, and other exotic means to store and release energy, we concluded that mechanical springs were a convenient and robust storage mechanism. To solve the problems of inefficiency and high holding force, we turned to a combined spring/linkage mechanism. Figure 10 depicts the geometry of a geared six-bar spring/linkage system that we have found to be surprisingly effective. Figure 11 shows a photograph of its mechanical implementation in both its compressed and uncompressed states. The leg extension is along the y-direction in Figure 10. Displacements in the y-direction induce, through the linkage, displacements in the linear spring along the x-direction. In effect, the linkage creates a non-linear spring from a linear spring. In addition, this concept can be practically implemented in a stiff structure with low internal friction.

The thrust force versus leg displacement relation for this mechanism can be determined as follows. From the geometry of Figure 10 we can derive an expression for y as a function of x

$$y = \sqrt{a^2 - (x-c)^2/4} + \sqrt{b^2 - (x-c)^2/4}, \qquad (3)$$

where the constants a, b, and c are defined in Figure 10. This equation can be solved for x:

$$x = c + \frac{\sqrt{2a^2(b^2+y^2) - (b^2-y^2)^2 - a^4}}{y}. \qquad (4)$$

If F_x denotes the spring force along the x-axis due to spring distension, and if F_y is the thrust force in the y-direction, then the principle of virtual work states that for an infinitesimal displacement of the mechanism, $F_x\,\mathrm{d}x = F_y\,\mathrm{d}y$. From this we obtain

$$\begin{aligned} F_y &= \frac{F_x}{\mathrm{d}y/\mathrm{d}x} = \frac{-k(x-l_0)}{\mathrm{d}y/\mathrm{d}x} \\ &= \frac{4k(x-l_0)}{x-c}\left[\frac{\sqrt{a^2 - \frac{(x-c)^2}{4}}\sqrt{b^2 - \frac{(x-c)^2}{4}}}{\sqrt{a^2 - \frac{(x-c)^2}{4}} + \sqrt{b^2 - \frac{(x-c)^2}{4}}}\right] \end{aligned} \qquad (5)$$

where k and l_0 are the spring's constant and undistorted length, respectively. An expression for F_y as a function of y can be obtained by substituting eq. (4) into eq. (5). For the particular case where $a = b$ (which represents the geometry of our prototype)

$$F_y = k\,y\left[\frac{(c-l_0) + \sqrt{4a^2 - y^2}}{\sqrt{4a^2 - y^2}}\right].$$

Figure 12 plots F_y versus y for the case where $a = b$, $(l_0 - c) = 1$, and the spring constant is normalized to $k = 1$. This figure shows the effective non-linear spring law realized by this compound mechanism.

The surprising utility of this linkage can be understood by comparing the shape of this graph with that of Figure 5(b). The maximum leg thrust is realized in the middle of the thrusting phase, while the thrust force at the onset of lift-off is quite low. This force/displacement profile substantially reduces the

Fig. 8. Photograph of the second generation hopper in the uncompressed state. The ruler in the photograph has a total length of 5 cm. The battery is not shown.

Fig. 9. Photograph of the second generation hopper in the compressed state. The ruler in the photograph has a total length of 5 cm.

likelihood of premature lift-off due to the shocks inherent in initial spring release. Furthermore, since the peak force realized during displacement is reduced, the motor's peak design torque is reduced as compared with the linear spring leg, i.e., this feature allows a smaller motor to recharge the thrust mechanism. Additionally, note that when this leg is nearly fully compressed, very little force is required to maintain the compressed state. Hence, after energy is stored in the leg, a surprisingly small amount of force is required to maintain the leg in its compressed state. This allows for a very small locking mechanism (see Figure 13).

Mechanically, the primary motor compresses the leg via a power screw. The screw is driven until it connects with a latching mechanism (see Figure 13), whereupon leg compression commences. The leg is compressed until a micro-switch is tripped. When the robot is ready to hop, a small amount of additional compression causes a mating wedge on the six-bar to release the leg latch. Figure 13 shows a detail of the latching mechanism at the moment when the power screw is engaging with the latch. Also shown in the figure is the bottom part of the six-bar mechanism and of the spring. The entire assembly is mounted at a roughly 50° angle with respect to the foot's

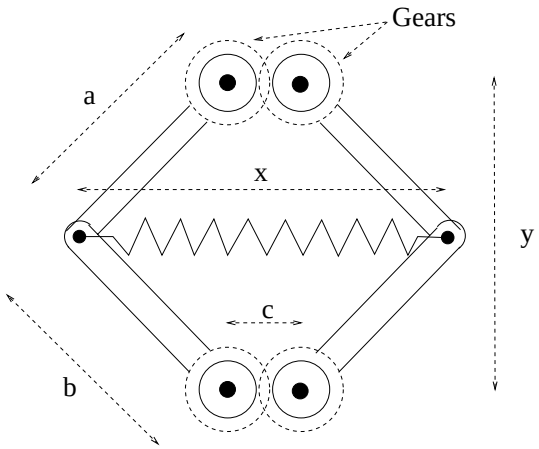

Fig. 10. Schematic diagram of the second generation energy storage linkage, a six-bar geared mechanism.

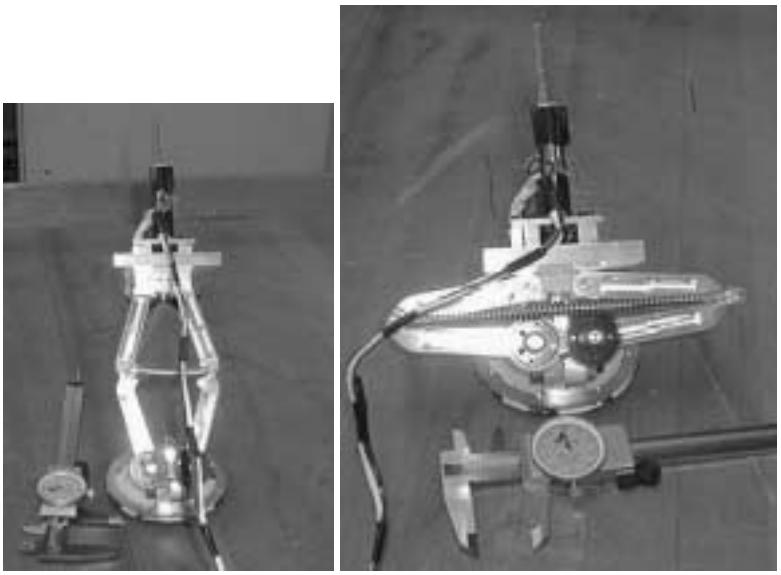

Fig. 11. Photographs of the second generation thrust leg: (a) uncompressed state; (b) compressed state. The self-righting mechanisms and crash cage are removed for clarity.

horizontal axis. This fixed take-off angle roughly optimizes the horizontal hopping distance over a wide variety of ground characteristics.

Experiments with this system have shown that this leg design realizes a 70% mechanical energy conversion efficiency, versus 20% for the first generation linear spring design. As shown in the experiments below, this high efficiency enables long hops.

6.2. The Active Steering Mechanism

To robustly and accurately point this system in a desired direction, as well as to point the on-board camera, the second generation device employs an active steering mechanism. The main robot structure is attached to the foot by a bearing that rotates about the vertical axis (Figure 14). When the leg reaches its maximum compression, a pinion gear that is driven by the primary motor engages with a ring gear that is rigidly attached to the foot. Rotation of the pinion controls the steering angle. Since the camera is attached to the upper body, steering can also implement panning of an on-board camera. Note that, because of the multiplexing required by our single motor design, steering is unidirectional.

6.3. Self-Righting Mechanism

The hopper will typically land in an unpredictable toppled configuration. Hence, an active mechanism was devised to

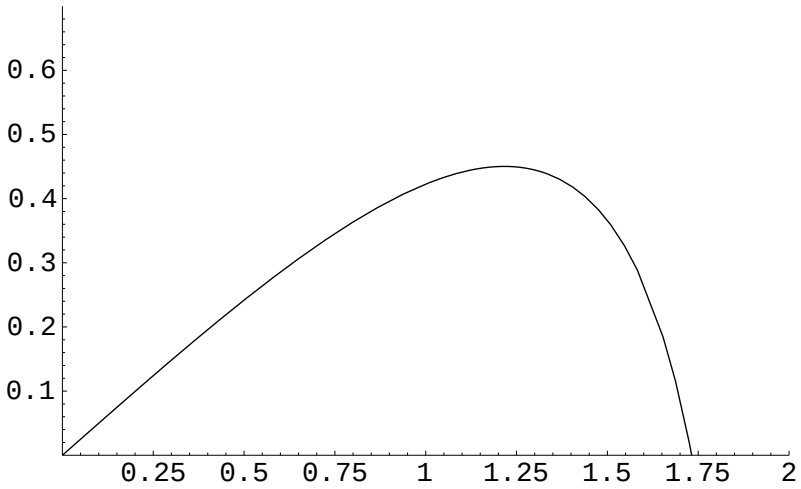

Fig. 12. Reaction force versus leg extension for the six-bar geared linkage (case $a = b$, and normalized spring constant).

Fig. 13. Photograph of latch mechanism.

bring the mechanism to an upright and stable posture. To cope with a large variety of possible landing configurations, a two-stage self-righting process and self-righting mechanism was designed. The outer profile of the hopper's crash cage is roughly a triangular prism. Hence, after a hop, the uncompressed system is very likely to come to rest on one of the prism's faces. During the *first phase* of the self-righting process, flaps (whose stored configurations make up part of two faces) open up, causing the hopper to roll onto its "back" face. A time elapsed photograph of one flap movement is shown in Figure 15. Note that the foot has a circular profile that facilitates this rolling process.

In the *second phase*, the rotation of a large flap (that is initially flush with the hopper's back face) forces the hopper toward an upright configuration. The leg compression phase is timed to coincide with this part of the self-righting process. By compressing the leg during this phase, the hopper's center of mass sympathetically shifts in a way to aid the uprighting process that is driven by the back flap's movement. The leg is compressed by the end of phase II, preparing the vehicle for subsequent hops. Mechanically, the coordination is done by driving the phase II process from the gears of the geared six-bar leg. With this two-phase process, the hopper can nearly always be brought to an upright position, in preparation for the next operational cycle. The hopper's broad foot combined with its low center of mass in the compressed state ensures that the upright posture is statically stable.

6.4. Operation Sequence

The main hopper subsystems have been outlined above. A key novelty of our design is its ability to drive all of these subsystems with a single motor. Like the first generation design, we use an overrunning clutch to allow opposite motor rotations to drive different operations. However, the second generation design cycles through more operations, and novel

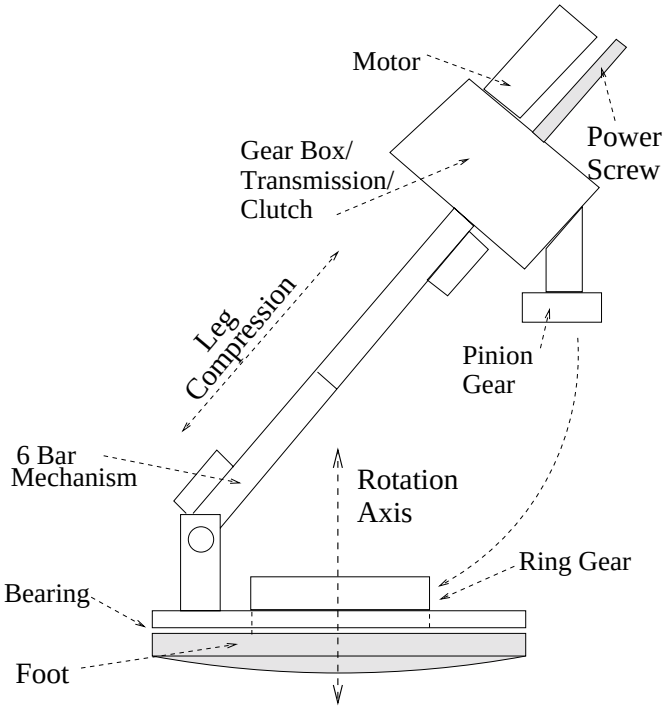

Fig. 14. Schematic diagram of the steering mechanism. The self-righting mechanism, crash cage, and several components are omitted for clarity.

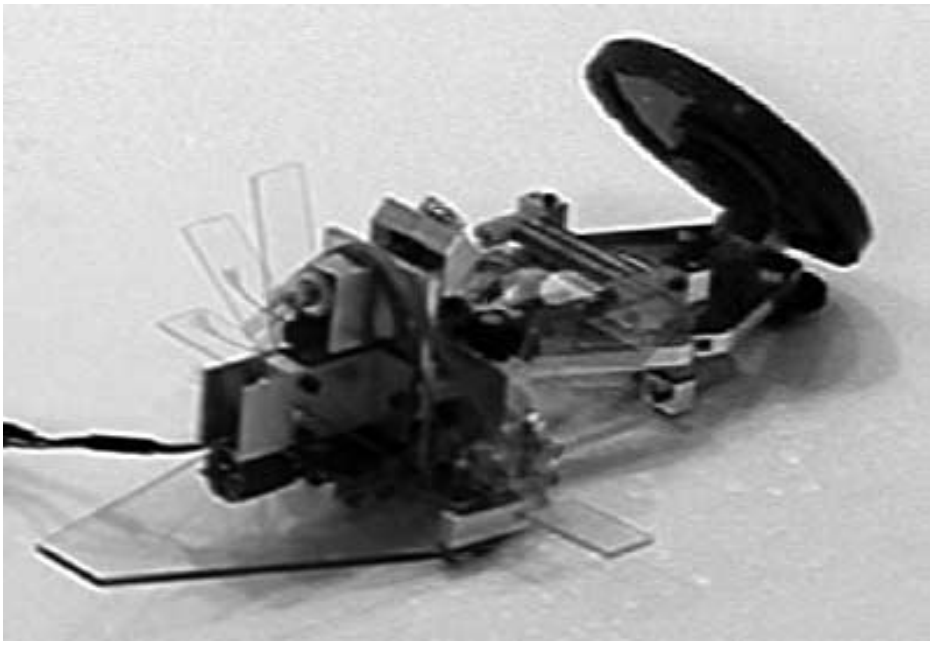

Fig. 15. Time elapsed photograph showing opening of one side flap during phase I of the self-righting operation. Note that side flaps open symmetrically. Only one flap is shown for simplicity. The crash cage is removed for clarity.

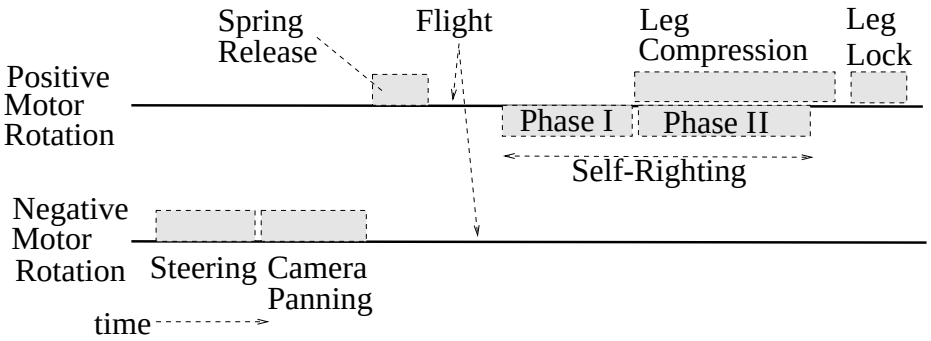

Fig. 16. Depiction of timing/phase of motor operations driven by the single primary motor.

timing mechanisms, mechanical logic, and couplers (whose presentation is beyond the scope of this paper) were introduced to coordinate the various actions. Figure 16 presents a timing diagram like that in Section 4.

7. Second Generation Experimental Results

We tested this device on a variety of surfaces. It typically jumps a horizontal distance of 1.8–2.0 m, and reaches a vertical height of ∼0.9 m during free-flight. In the lower gravity environment of Mars (one of the primary opportunities for this vehicle), this performance would translate into a horizontal movement of ∼6.5–8.0 m and vertical ascent of ∼3 m. This system could potentially overcome physical obstacles of considerable size. Note that, as gravity becomes lower and lower, robot jumpers gain considerable ability to overcome large obstacles, whereas the obstacle surmounting capability of wheels does not increase with lower gravity.

Figures 17–21 show digitized images from a video that captures a complete cycle of the hopper's operation. The cycle begins with the robot in a posture like that of Figure 9. After steering to the intended direction, the leg is released. Figure 17 shows a blurry image of the device during free-flight.

During this particular trial, the device came to rest on its side after touchdown (Figure 18). Figure 19 captures an instant during the first phase of the self-righting process, where the side flaps unfold to position the hopper on its back. Figure 20 shows that the hopper has rolled onto its back by the end of the first self-righting phase.

Figure 21 occurs near the beginning of the second self-righting phase, while Figure 22 occurs near the end of this phase. The back flap is pushing the hopper toward a standing position. The progress toward a standing posture is aided by the leg compression, which moves the mass center in a sympathetic manner.

An mpeg movie of the entire sequence can be viewed at http://robotics.caltech.edu/∼jwb/hopper30.mpg, while the QuickTime version can be found at http://robotics.caltech.edu/∼jwb/hopper15.mov.

7.1. Comparison with Wheeled Rover

It is interesting to compare the performance of our second generation prototype with that of the Nanorover, since they address similar exploration missions. We do not intend to suggest with this comparison that the Nanorover is anything but an excellent vehicle. Instead, our comparison suggests that our proposed hopper is a viable alternative that could profitably be pursued for some applications. The comparisons are based on data collected from our experiments and published data for the Nanorover (Welch, Wilcox, and Nasif 1998). Based on the data collected from experiments with our prototype, we can summarize our quantitative comparisons relevant to Martian applications in Table 1.

With reference to mass and power consumption, the two devices are essentially equal. In fact, the latest Nanorover prototype has 1 kg mass, whereas the second generation prototype has approximately 1.3 kg mass. To compare power, we consider the distance covered by a single jump of the hopper, i.e., 8 m on Mars. The Nanorover has a maximum power feed of 1 W, but requires less for nominal travel—of the order of 350 mW. With the assumption that no obstacles need be avoided, the Nanorover will consume 93 W s^{-1} for an 8 m traverse, excluding sensing and communication. The hopper draws 4 W of power for 30 s during leg compression, approximately 100 mW during 50 s of self-righting, and a negligible amount for steering. The total energy required for the 8 m hop is approximately 125 W s^{-1}. Taking Nanorover obstacle avoidance maneuvers into account, the energy consumption of the two will be essentially equal.

Table 1. Comparison between Nanorover and Hopper

	Mass (kg)	Time (min)	Power (W s^{-1})	Obstacle (m)
Nanorover	1	4.3	93	.09
Hopper	1.3	1.5	125	4.5

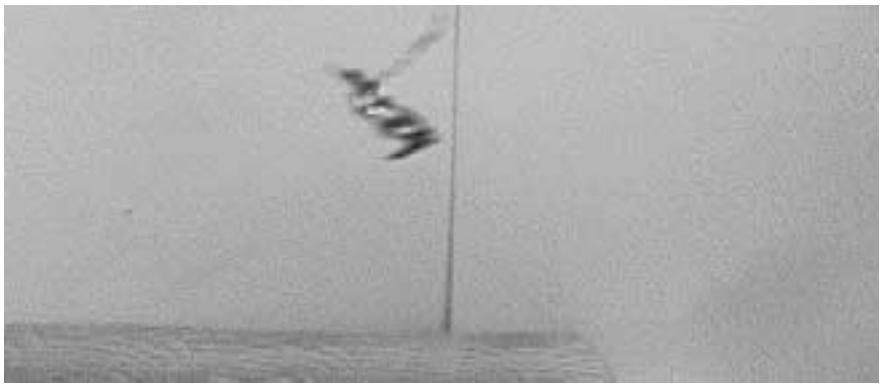

Fig. 17. Flight phase.

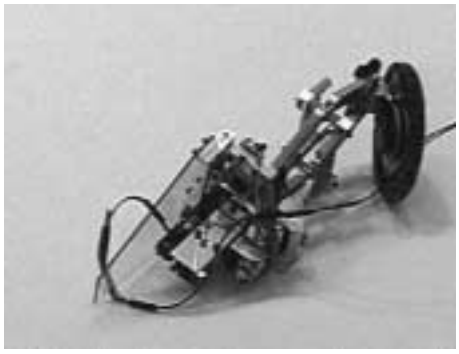

Fig. 18. Landing configuration.

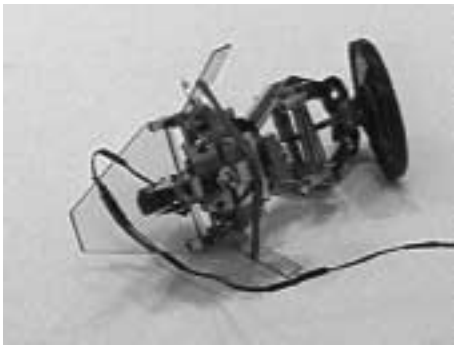

Fig. 19. First phase of self-righting sequence. The side flaps are opening.

However, when comparing performance, the two devices are significantly different. Based on its maximum speed of $3\,\mathrm{cm\,s^{-1}}$, the Nanorover would require at least 4.3 min to travel an 8 m path, making the unrealistic assumption that no time is spent on obstacle avoiding maneuvers. On Mars, our hopper can travel this 8 m distance in a single hopping cycle, whose duration (including thrust charge, steering, and self-righting) is approximately 1.5 min. Hence, our hopper is effectively three times as fast. Similarly, based on the Nanorover's 6 cm wheel diameter, it can only avoid approximately 9 cm tall abrupt obstacles at best. On Mars, the hopper could leap over obstacles as high as 3 m—nearly 50 times higher than the Nanorover's capability.

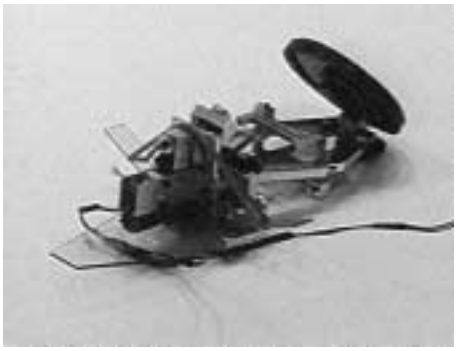

Fig. 20. Posture at the end of self-righting phase I.

8. Generation Three: The Wheeled Hopper

The second generation device answered the question: how much mobility can one obtain by a single motor? It also practically confirmed the utility of several key mechanical design elements for our minimalist approach—efficient energy storage devices and active self-righting. From the point of view of science acquisition, this system had two main shortcomings as follows.

1. The lack of an adjustable take-off angle. An adjustable take-off would enable the robot to better pinpoint its landings and to tailor its aerial trajectories for specific obstacles. Vertical take-offs might even enable panoramic camera viewpoints. Note that the take-off angle is the elevation angle with which the robot takes off at the beginning of a jump.

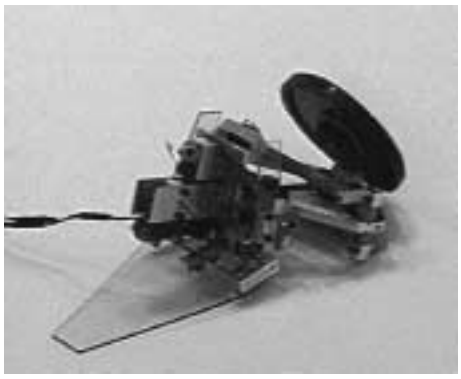

Fig. 21. Second phase of the self-righting sequence.

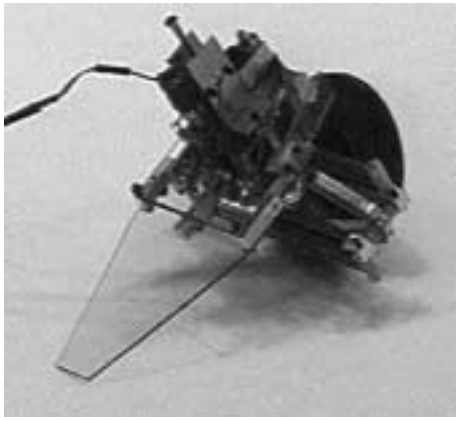

Fig. 22. Second phase of the self-righting sequence.

2. The lack of fine mobility. The lack of wheels, treads, or other means to implement fine adjustment of the robot's position on the terrain limits its science gathering ability. For example, once the vehicle self-rights after a jump, it cannot locally maneuver to precisely position a scientific instrument.

The third generation device contained components that addressed two of these shortcomings. It retained the six-bar thrusting mechanism (although with a new compression driver), while adding two driven wheels and a mechanism to adjust the take-off angle. This system also incorporated realistic on-board computation and wireless communication. We did not attempt to solve the self-righting problem for this vehicle, saving this issue for the next generation (see Section 10).

Figure 23 shows the hopper in the take-off position, and we use this figure to point out the main mechanical details of the new prototype. In the picture, springs, wheel motors, electronics, and protection cage have been removed for clarity. The main mechanical component of the hopper is the gear-box to compress the thrusting springs. In the second generation, the spring was compressed by a rigid power screw. In this prototype, the spring is compressed by winding a cable on a capstan. The cable's retraction compresses the spring.

The third wheel at the rear of the hopper is a passive caster for stability. This wheel is attached to the output of a four-bar mechanism, whose motion is driven by the take-off angle adjustment system. In the compressed configuration, the robot must be able to drive around. To enable this, the foot is tucked up under the vehicle, while the rear wheel is lowered to a functional position. In preparation for launch, the foot is lowered while the rear wheel is simultaneously raised by the coupled action of the four-bar. Once the foot contacts the ground, continued movement of the angle adjustment system increases the take-off angle. In this prototype, the take-off angle could be continuously adjusted from 0° to $\sim 85^\circ$. This take-off-angle and wheel raising system is powered by the motor via a shaft that engages when the leg is compressed. The driving motor is multiplexed so that one direction of travel compresses and releases the leg, while the other direction of movement drives the take-off angle control mechanism. Figure 27 shows the extended linkage attached to the rear of the gear-box, and the cable used to compress the leg. The twin wheels below the gear-box are powered by two independent motors, visible in Figure 26.

The wheels shown in the photographs are clearly not intended for use in rough terrain. Instead, they allow conceptual and functional tests. In fact, as we discuss in Section 10, our future designs are not based on wheels. The hopper's foot is elliptical to support different take-off positions. Fine motion control is provided by the two front wheels, which can steer the robot to the desired hopping direction, to locally maneuver for purposes of reaching suitable scientific targets, or to traverse relatively benign terrains. The hopper drives while its leg is in the compressed configuration, as shown in Figure 24. However, we are considering the possibility of cruising also in the extended configuration to use the elliptic foot as a scoop to collect terrain samples, as shown in Figure 25. Figure 25 is a side view of the complete hopper, with clearly visible the spring compression cable, the rear capstan, and the antenna for data communication.

In order to realistically assess the practical impact of a full on-board electronics suite, the component packing geometry and overall system mass, this prototype is equipped with an electronic package, surrounding the gear-box, providing motor control, programmability, and communication with a remote operator. The electronic control is provided by two micro-controller boards each equipped with a PIC CMOS microprocessor, motor controller and power circuits, communication ports, and analog/digital signal acquisition. The boards communicate with each other using the I^2C protocol and with the operator's PC via an RF connection. Each board consumes $\sim$0.35 W, excluding motor and science instruments. Additionally, the major board components have power-down features to conserve energy. Power is provided

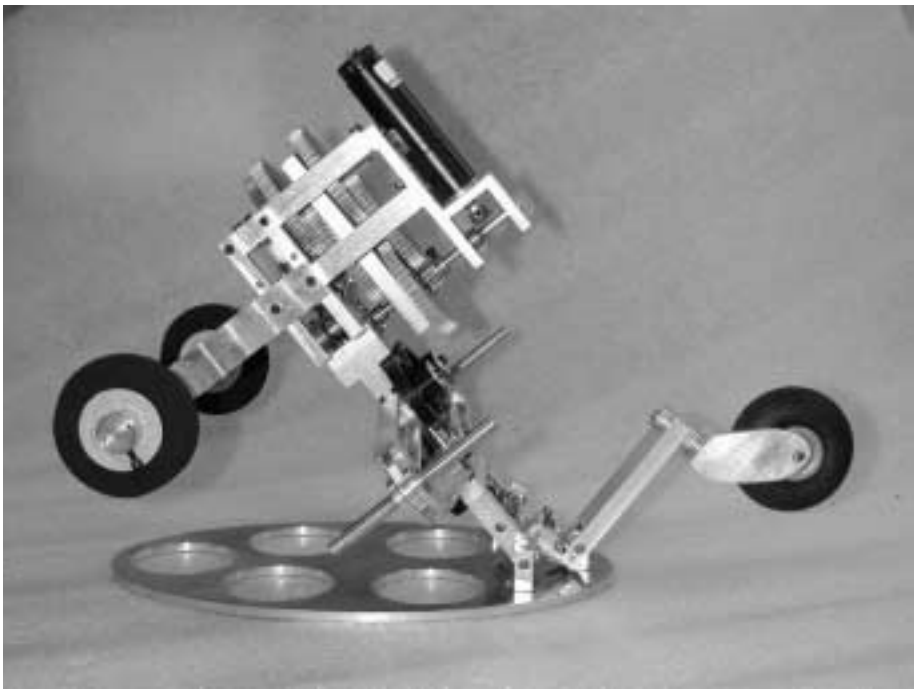

Fig. 23. The third generation hopper in take-off position.

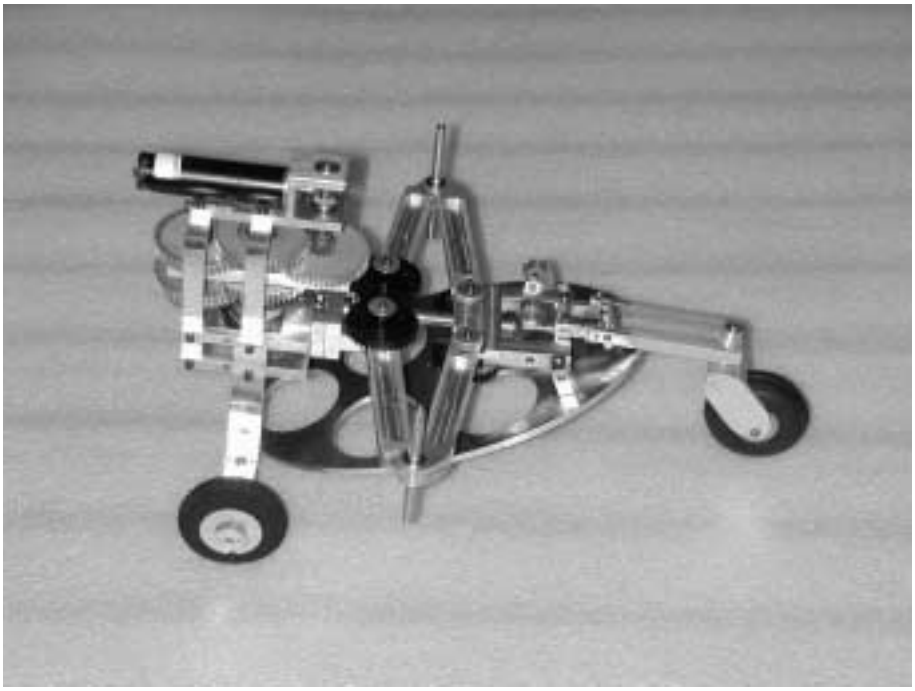

Fig. 24. The third generation hopper in the compressed cruising configuration.

Fig. 25. The third generation hopper in the extended cruising configuration.

by four primary 12 V batteries. The instrument suite is currently simulated by a video micro-camera, mounted in front of the hopper, broadcasting images directly to operator's PC. The crash cage added to the hopper to protect the electronics during crash landing, is clearly visible in Figure 27.

The front view of the complete hopper is shown in Figure 26; the TV camera simulating a scientific instrument is visible in the center of the hopper body. The operator station for teleoperating the hopper is shown in Figure 27. The operator station consists of a laptop computer equipped with two radio links: a full duplex channel for command and data exchange with the hopper, and a TV link to download images taken by the on-board camera. The computer screen shown in Figure 27 displays a window of the hopper camera imaging the computer mouse, and the command windows, with buttons for simple commands, such as *move forward* and *hop*. Using the buttons in the command window, the operator can control the hopper motion, initiate a hop, and acquire data about wheel position and take off angle.

Figure 28 shows one experiment to verify the operational capabilities of the hopper in a simulated terrain. During this first capability test, the hopper was able to drive on a flat carpeted area and easily hopped over rocks approximately 30 cm high, all under remote operator control. In practice, the rearward positioning of the caster limits the vehicle's maneuverability, especially in sandy terrains. We briefly address this issue in Section 10.

9. Localization and Sensing

In order to navigate an unknown terrain, the hopping robot must be equipped with suitable sensors and localization algorithms to identify, after a landing, its current position. We are in the process of selecting a suitable sensor suite that could fit the volume and size constraints of the robot, and that could support the identification of its final rest position after a jump. The sensors we are investigating are divided into two groups: dynamic and vision. To the first group belong accelerometers and gyros, but also contact sensors to measure the position of the rock impacts on the robot body during landing. We have verified in simulation that, if such sensors were

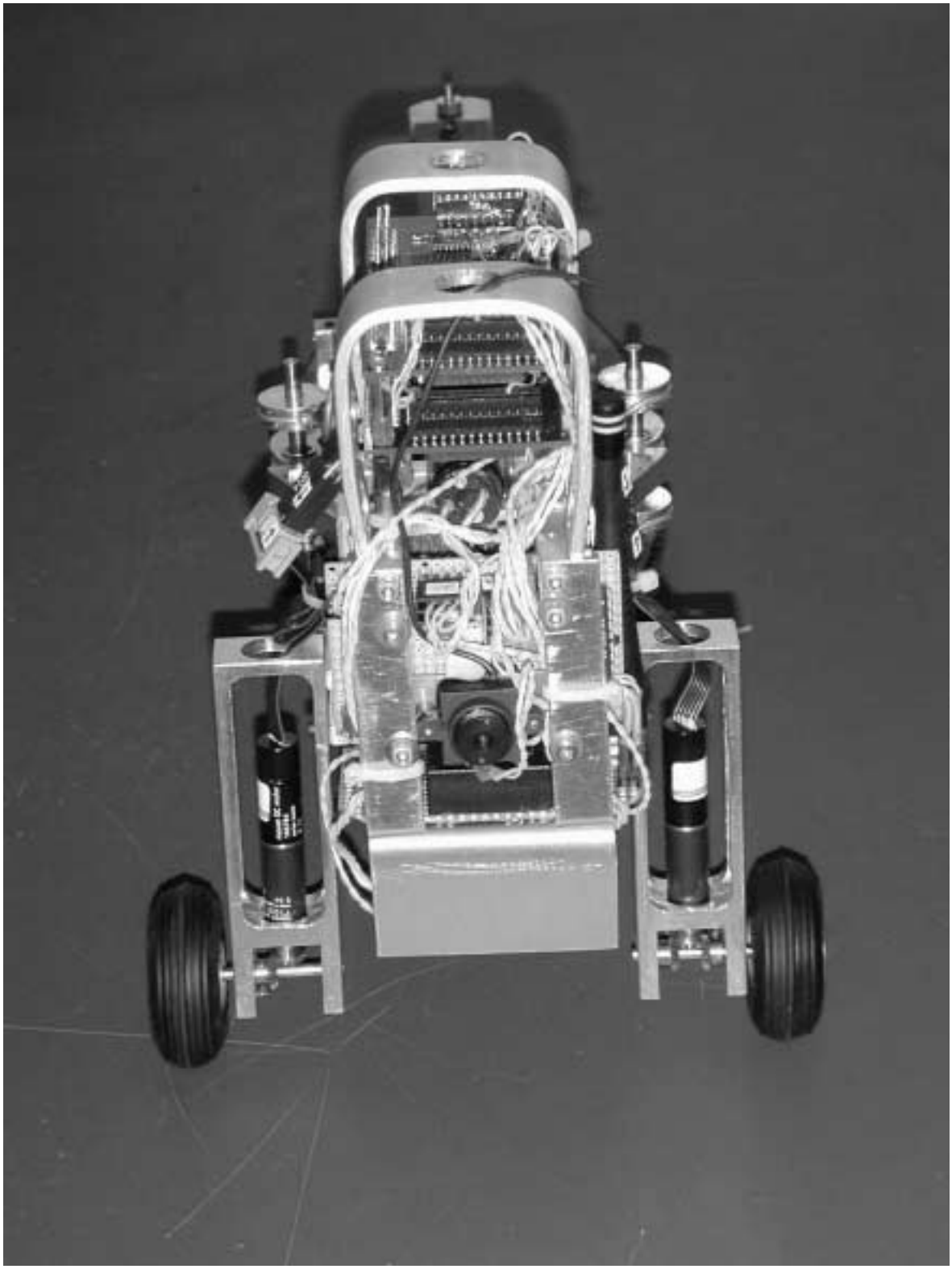

Fig. 26. Front view of the third generation hopper.

Fig. 27. The third generation hopper and its control station.

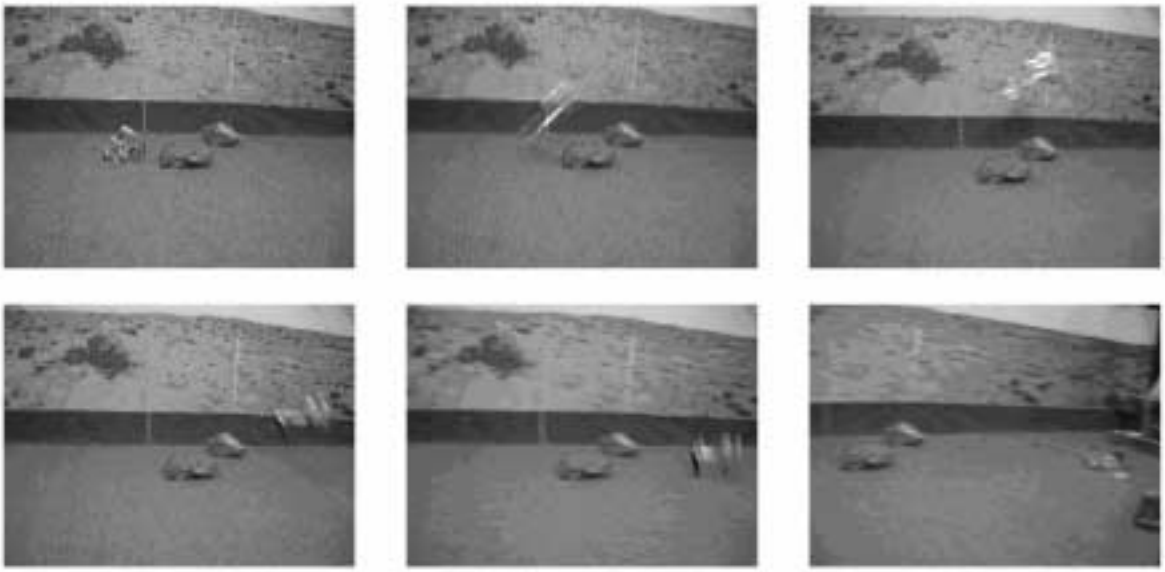

Fig. 28. Snapshot of the third generation hopper going over a rock.

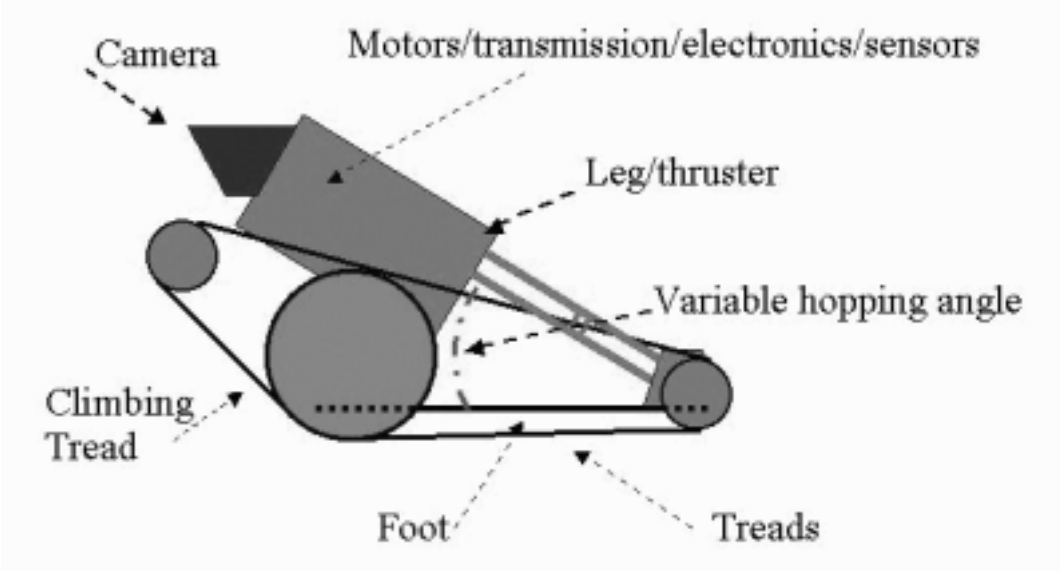

Fig. 29. Schematic diagram of the fourth generation concept.

available, we could reconstruct "a posteriori" the trajectory of the robot and identify with reasonable precision the final position of the robot. However, it is obvious that this approach leads to an unbound position error, if the initial estimate of the starting location of the jump is not known accurately. For this reason it is necessary to have an "absolute" position measurement of the type given by a vision sensor. Because of the physical constraints of the hopping robot, the vision system must be very compact, rugged and with a wide field of view. We are investigating the use of omnidirectional lenses, which combine small size and robustness with panoramic vision. By using epipolar geometry, we are also in the process of developing a stereo vision algorithm for a single omnidirectional lens, that would take advantage of the known displacement of the lens during the compression of the jumping mechanism. Thus, by resetting the trajectory estimation provided by the dynamic sensors with the vision system, we should be able to provide the hopper with reliable self-localization, and proceed to develop more advanced planning features.

10. Conclusion

In this paper we have explored a novel jumping paradigm which can potentially enable small vehicles to overcome significant obstacles in unstructured terrain. Additionally, we have developed an approach whereby such hopping can be implemented with a small number of actuators. We have also introduced several novel mechanisms to enable our paradigm. Our second generation hopper has offered surprising capability and reasonable efficiency in a small package that contains a single actuator. We have verified in our third generation that a small jumping system can also deploy wheels for fine mobility, control its jumping take-off angle, while also containing sufficient on-board computing and communication capability to carry out realistic tasks.

We are currently developing a fourth generation device which combines the leg thrusting mechanism of generations two and three, with the take-off angle control of generation three, the self-righting capability of generation two, and two treads (instead of wheels) for fine mobility (see the schematic diagram in Figure 29). The treads provide more stable maneuvering in soft terrain, which is a problem of the caster design in generation three. We hope that this system and its future versions will offer a useful alternative mobility platform for low-cost operations in remote terrain.

There are clearly several avenues of future work. Our second generation design achieved significant hopping distances, good efficiency, and robust steering. While its self-righting ability has been successful in our trials, we currently have no proof that the vehicle can self-right itself in all possible terrains with all possible contact conditions. This is clearly a serious issue that merits further attention. Furthermore, extending the self-righting concept to more complicated vehicles will require additional analysis. From the practical point of view, the use of more exotic structural materials (such as carbon-fiber composites) and exotic energy storage schemes should reduce the size and weight of future prototypes. Finally, the jumping/hopping paradigm poses several challenging issues in the development of navigation and sensing algorithms.

Acknowledgments

This work was supported by the JPL, California Institute of Technology (Caltech), under contract with NASA. This work

was also partially funded by a grant from the National Science Foundation through the Center for Neuromorphic Systems Engineering at Caltech, grant NSF9402726. The authors thank Andy Tretten, Matt Heverly, Jeff Gensler, Eric Hale, Nathan Schara, Steve Schell, Ed Barlow and Sawyer B. Fuller for their design and fabrication support, and Samad Hayati and Neville Marzwell of JPL-NASA for their financial support and encouragement.

References

Bares, J., Hebert, M., Kanade, T., Krotkov, E., Mitchell, T., Simmons, R., and Whittaker, W. 1989. Ambler: An autonomous rover for planetary exploration. *IEEE Computer* 22(6):18–26.

Bares, J., and Wettergreen, D. 1999. Dante II: Technical description, results, and lessons learned. *International Journal of Robotics Research* 18(7):621–649.

Berkemeier, M. D., and Fearing, R. S. 1998. Sliding and hopping gaits for the underactuated acrobot. *IEEE Transactions on Robotics and Automation* 14(4):629–634.

Bhattacharya, S., and Agrawal, S. K. 2000. Spherical rolling robot: A design and motion planning study. *IEEE Transactions on Robotics and Automation* 16(6):835–839.

Bicchi, A., Balluchi, A., Prattichizzo, D., and Gorelli, A. May 1997. Introducing the sphericle: An experimental testbed for research and teaching in nonholonomy. In *IEEE International Conference on Robotics and Automation*, San Diego, CA.

Budenske, J. R., Dvorak, M., Gini, M., Krantz, D. G., Li, P. Y., Malver, F., Nelson, B., Papanikolopoulos, N., Rybski, P. E., Stoeter, S. A., Voyles, R., and Yesin, K. B. April 2000. A miniature robotic system for reconnaissance and surveillance. In *IEEE International Conference on Robotics and Automation*, San Francisco, CA, pp. 501–507.

De Luca, A., and Oriolo, G. May 1998. Stabilization of the Acrobot via iterative state steering. In *IEEE International Conference on Robotics and Automation*, Leuven, Belgium, pp. 3581–3587.

Fiorini, P., Hayati, S., Heverly, M., and Gensler, J. March 1999. A hopping robot for planetary exploration. In *Proceedings of IEEE Aerospace Conference*, Snowmass, CO.

Hauser, J., and Murray, R. M. 1990. Nonlinear controllers for non-integrable systems: the Acrobot example. In *American Control Conference*, pp. 669–671.

Kaplan, M. H., and Seifert, H. 1969. Hopping transporters for lunar exploration. *Journal of Spacecraft and Rockets* 6(8):917–922.

Koditschek, D. E., and Bühler, M. 1991. Analysis of a simplified hopping robot. *International Journal of Robotics Research* 10(6):587–605.

Li, Z., and Montgomery, R. 1990. Dynamics and optimal control of a legged roboti in flight phase. In *IEEE International Conference on Robotics and Automation*, Cincinnati, OH, May, pp. 1816–1821.

Lorigo, L., Paul, C., Brooks, R., McLurkin, J., and Moy, M. 1997. Autonomy for Mars exploration. In *Workshop on Planetary Rovers at IROS'97*, Grenoble, France, 7–11 September.

Mishkin, A., Morrison, J., Nguyen, T., Stone, H., and Cooper, B. 1998. Operations and autonomy of the Mars Pathfinder Microrover. In *IEEE Aerospace Conference*.

Oberth, J. 1959. *The Moon Car*, Harper and Brothers, New York.

Raibert, M. H. 1986. *Legged Robots that Balance*, MIT Press, Cambridge, MA.

M'Closkey, R. T., and Burdick, J. W. 1993. Periodic motion of a hopping robot with vertical and forward motion. *International Journal of Robotics Research* 12(3):197–218.

Seifert, H. S. 1967. The lunar pogo stick. *Journal of Spacecraft and Rockets* 4(7):941–943.

Shigley, J. E., and Mischke, C. R. 1989. *Mechanical Engineering Design*, McGraw-Hill, New York.

Spong, M. W. February 1995. The swing up control problem for the Acrobot. *IEEE Control System Magazine* pp. 49–55.

Volpe, R. August 1999. Personal communication.

Welch, R., Wilcox, B., and Nasif, A. 1998. Nanorover for Mars. *Space Technology* 17(3–4):163–172.